Soft Matter

Correlation of Hierarchical Structure and Rheological Behavior of Polypseudorotaxane Gel Composed of Pluronic and β-cyclodextrin

Journal:	*Soft Matter*
Manuscript ID	SM-ART-03-2020-000406.R2
Article Type:	Paper
Date Submitted by the Author:	05-May-2020

Complete List of Authors:	Shih, kuo-chih; Nationnal Taiwan University, Agricultural Chemistry Su, Chien-You; National Chung Cheng University, chemical engineering Chang, Shing-Yun; National Taiwan University, Dept. Agricultural Chemistry Jensen, Grethe ; University of Delaware, Chemical and Biomolecular Engineering; National Institute of Standards and Technology, Center for Nuetron Research Hua, Chi-Chung; National Chung Cheng University, Department of Chemical Engineering Nieh, Mu-Ping; University of Connecticut, Chemical and Biomolecular Engineering; University of Connecticut, Polymer Program, Institute of Materials Science Lai, Hsi-Mei; Nationnal Taiwan University, Agricultural Chemistry

Correlation of Hierarchical Structure and Rheological Behavior of Polypseudorotaxane Gel Composed of Pluronic and β-cyclodextrin

Kuo-Chih Shih[1], Chien-You Su[2], Shing-Yun Chang[1], Grethe Jensen[3, 4], Chi-Chung Hua[2], Mu-Ping Nieh[5, 6, 7] and Hsi-Mei Lai[1*]*

[1] Department of Agricultural Chemistry, National Taiwan University, Taipei, 10617, Taiwan

[2] Department of Chemical Engineering, National Chung Cheng University, Chiayi County 62102, Taiwan

[3] Department of Chemical and Biomolecular Engineering, University of Delaware, Newark 19716, Delaware, USA

[4] National Institute of Standards and Technology (NIST) Center for Neutron Research (NCNR), Gaithersburg 20899, Maryland, USA

[5] Institute of Materials Science, [6] Department of Chemical and Biomolecular Engineering [7] Department of Biomedical Engineering, University of Connecticut, Storrs 06269, Connecticut, USA

* Corresponding authors. Tel.: +1 8604868708 (M.-P. Nieh); tel.: +886 233664816, fax: +886 23633123 (H.-M. Lai). E-mail addresses: mu-ping.nieh@uconn.edu (M.-P. Nieh), hmlai@ntu.edu.tw (H.-M. Lai).

Abstract

We have identified the hierarchical (primary, secondary, tertiary and quaternary) structures of a polypseudorotaxane (PPR) gel composed of Pluronic F108 and β-cyclodextrin system to be β-cyclodextrin crystalline, lamellar sheets, lamellar stacks and "grains", respectively. Correlation between the rheological properties to the proposed structures under shear flows was rationalized. Alignment of lamellar stacks and reorganization of grains boundaries under shear flows were investigated by rheo-SANS, small angle X-ray scattering and small-angle light scattering. The relaxation of highly aligned lamellar stacks is slow (> 2 h) after flow cessation compared to that of the regrouped grains (a few minutes). The main contribution to thixotropic behavior is likely from the faster relaxation of the reorganized grains containing highly oriented lamellar stacks. The comprehensive understanding of structure-function relationship of PPR gel will facilitate the rational design for its applications.

Keywords: Polypseudorotaxane, Small-angle Neutron Scattering (SANS), Small-angle Laser Scattering (SALS), Rheology, Thixotropy.

Introduction

Pluronics (PLs), also known as poloxamers, represent a unique class of non-ionic amphiphilic triblock copolymers composed of a central hydrophobic poly(propylene oxide) (PPO) block and two end hydrophilic poly(ethylene oxide) (PEO) blocks. PLs form a variety of self-assembled structures in selective solvents depending on the molecular architecture, the concentration of PL and temperature of the system.[1] PL micelles can also be found above the critical micelle concentration (CMC) at a specific temperature.[2, 3] A transparent gel with shear-thinning[4] and thermoreversible properties[5] can also be obtained with increased temperature or concentration to above the critical gelation temperature (CGT) or critical gelation concentration (CGC). Where CGT and CGC is the minimum temperature or concentration for PL to form gel at specific concentration or temperature, respectively.

A supramolecular assembly, polypseudorotaxane (PPR), has been reported when cyclodextrin (CD) is introduced in the system where several CD molecules are thread by the PL chains forming a rigid rod-like structure.[6] The self-assembly is driven enthalpically through host-guest interaction between the PPO segments and the hydrophobic cavity of CD.[7] The unique

structure and rheological behaviors are compared against those in absence of CD. The PL self-assembles differently with various compositions of CD introduced to the system. At lower β-CD-to-PL ratio, β-CD can associate with PL resulting in dissolute[8-10] or swollen PL micelles.[11] As β-CD-to-PL ratio increases, PPR can form resulting in morphologies of hollow sphere,[12] rod-like,[9, 13] lamellae (platelet)[11, 14, 15] or lamellar stacks.[13, 15, 16] When sufficient amount of CD is introduced to the system, sol-gel transition,[17-23] thermoreversibility[17-19] and thixotropy [20, 22, 24] are attainable. In this study, we focus on understanding the origin of thixotropic behavior, which has not been fully comprehended.

We intend to provide the insight into the correlation of hierarchical structures with thixotropy, where viscosity increases with equilibrating time after shear. For this system, thixotropic behavior was found in the soft-gel region with sufficient β-CD concentration. This can be achieved by dispersing β-CD in 24% citric acid (CA) aqueous solution resulting in an order of magnitude of enhancement in β-CD solubility compared to that in pure water.[13] A preliminary study mapping out the the gelation behavior of the β-CD/PL system was conducted to evaluate the effects of β-CD and PL concentrations as shown in Figure S1.

Previous reports have shown that the thixotropy in β-CD/PL system[25, 26] is related to the microstructures. Because of the unique rheological property, PPR gels have recently been suggested as a potential injectable hydrogel for local tumor chemotherapy.[27] However, the origins of thixotropy for PPR gels remains little explored to date.[6, 28, 29] Nevertheless, thixotropy is generally considered as a reversible mechanotropic property occurring as a consequence of structural reorganizations at the microscopic scale.[30] Therefore, this study investigates on the correlation between the detailed (multiscale) structures and thixotropy of a model PPR gel under various flow conditions using a combination of light/X-ray/rheo-neutron (full range) scattering and rheological analysis schemes. The result reveals, for the first time, the existence of complex hierarchical microstructure of the PPR gel that responds to varying flow rate or strength and produces thixotropic feature of distinct origins.

Experimental Section

Materials

PL F108 (EG_{133}-PG_{49}-EG_{133}, Mw 14,600 g/mol) was purchased from BASF (Florham Park, New York, USA). β-CD (purity ≥ 97%) was obtained from Sigma-Aldrich (St. Louis, MO,

USA). Deuterium oxide (D_2O, D, 99.9%) was purchased from Cambridge Isotope (Andover, MA, USA). All chemicals used in the present study were of analytical grade.

Sample Preparation

Sample preparation methods have been described in a previous study.[13] Briefly, a 20% (w/v) β-CD stock solution was prepared in 24% CA solution. F108 pellet (150 mg) was first dissolved in the 24% CA solution (350 μL) followed by mixing with β-CD stock solution (500 μL). The solution will be stored at 6 ± 2°C for 12 h and at 25°C for an additional 24 h before all subsequent measurements. The final model PPR gel contained 15% F108 and 10% β-CD. A control sample was also prepared by the above-mentioned protocol in absence of β-CD (i.e. dissolving 150 mg of F108 in 850 μL of 24% CA solution) as a reference.

Gel determination of the β-CD/F108 mixture

Samples were prepared at β-CD and F108 concentrations ranging from 0-20 and 0-40% (w/v), respectively, to provide the complete survey of the gelation behavior of the system (Figure S1). The gel determination was performed by visual observation of the fluidity of the inverted test tube and the rheological property was further characterized using a rheometer. The sample that retained on the bottom of the tube for 20 s after inversion was referred as a hard gel. The fluidic sample was performed by using AR 2000ex rheometer (TA Instruments, New Castle, England) equipped with a parallel plate

(40 mm diameter, gap = 800 μm) and a solvent trap at 25°C. The oscillation strain sweep at 1 Hz was performed with the strain ranged from 0.001 to 5% to determine the linear viscoelastic region (LVER). Then, the oscillation frequency sweep was measured with the frequency increased in an exponential manner from 0.04 to 10 Hz with a chosen strain in LVER. Sample with the storage moduli (G') higher than the loss moduli (G'') was referred as a soft gel, otherwise was referred as a liquid. The PPR gel in this study appeared to be soft gel and its viscoelastic properties is shown in Figure S2.

Small/Wide-angle X-ray Scattering (SWAXS)

The SWAXS experiments were performed on the beamline 23A1 at the National Synchrotron Radiation Research Center (NSRRC, Hsinchu, Taiwan) in Taiwan. Samples were loaded in the standard solution cell and Kapton films were used as the cell window. The data were collected using photons with an incident energy of 15 keV (incident wavelength $\lambda = 0.827$ Å) and sample-to-detector distance of ~3500 mm. The SAXS scattering signals were collected by a Pilatus-1MF detector bearing a 981 × 1043 pixel resolution. This setup provides a q-range from 0.006 to 0.38 $Å^{-1}$. The WAXS scattering patterns were recorded by a CMOS flat panel X-ray detector (C9728DK with an area of 52.8 mm^2) at a sample-to-detector distance of 139 mm. The scattering intensity was put on the absolute scale by a secondary PE standard which has been calibrated by the scattering from water.

Small-angle Light Scattering (SALS)

The SALS apparatus was described elsewhere.[31] A 2 mW He-Ne laser with a wavelength (λ) of 632.8 nm and a beam diameter of 0.8 mm was used as the incident light which is guided through a spatial filter to enhance the beam homogeneity. Samples were loaded in a quartz cell of 2 mm path length to prevent multiple scattering. The PPR gel in quiescent state as well as after a short-term mild stirring was measured. The exposure time for each frame was set to be 20 s. The scattering pattern of a water sample was utilized for background subtraction. Data were collected in a range of scattering

angles θ = 2-20° which correspond to a q (defined as $\frac{4n\pi}{\lambda}\sin\left(\frac{\theta}{2}\right)$, n being the refractive index of the material examined) range of $6 \times 10^{-5} - 4.5 \times 10^{-4}$ Å^{-1}. All scattering patters were measured at 25.0 ± 0.1°C. The sample are measured in quiescent state as well as measured after the sample has experienced a mild stirring.

Confocal Laser Scanning Microscope (CLSM)

The PPR gel was stained with Nile Red (NR) before the image was taken by using a CLSM. 100 μL of 1% NR acetone solution was added in an amber vial and the resulting solution is dried with N_2 to obtain 1 mg of NR in the vial. Afterward, 1 mL of PPR gel was added in the vial and shaken overnight for NR to dissolve in the PPR gel. A fluorescence image of the NR-containing PPR gel on a cover slip was recorded using an inverted CLSM (Nikon A1R Spectral Confocal, Japan) equipped with oil lens (Plan Apo 60X/1.4 Oil, Nikon, Japan). The measurement was carried out under ambient conditions with an excitation wavelength of 561 nm and emission wavelengths of 575 - 625 nm, respectively. The particle sizes were analyzed by the Fiji ImageJ software.[32]

Static Light Scattering (SLS) / (Depolarized) Dynamic Light Scattering (DDLS/DLS)

SLS, DDLS and DLS measurements were performed on a laboratory-built instrument as described elsewhere.[31, 33, 34] DDLS is set up similarly to DLS, except for an analyzer (i.e., a polarizer) being placed before the detector to depolarize the scattered beam. The incident light is a 34 mW polarized He−Ne laser with the wavelength (λ) of 632.8 nm. A cylindrical quartz cell (Hellma, 540.111, Germany) is used to contain the sample solution with 2 mL in volume, with a cap that prevents solvent evaporation during the entire experiment. It should be noted that all measurements were conducted at 25.0 ± 0.1°C for a range of scattering angles θ = 30−140° in quiescent state (before and after shear) instead of “under shear flow”. Details of static, dynamic, and depolarized dynamic light scattering (SLS/DLS/DDLS) analysis schemes can be found in prior work.[31, 33, 34]

Rheo-SANS Measurement

Rheo-SANS experiments were conducted in the 1-3 (flow-vorticity) and 2-3 (velocity gradient-vorticity) plane, respectively (Scheme S1), at the NGB 30 m SANS instrument located at the National Institute of Standard and Technology (NIST) Center for Neutron Research (NCNR).[35] Data reduction was performed on the IGOR Pro software with the NCNR data reduction macro.[36] The neutron wavelength was 6 Å with a wavelength spread, $\Delta\lambda/\lambda$ of 12.0%. A detector distance of 6 m was used to cover a q range from 0.008 to 0.18Å^{-1}. Couette geometry was used and composed of a titanium moving inner bob and stationary outer cup ($R_1 = 27.0\,\text{mm}$; $R_2 = 29.0\,\text{mm}$). A solvent trap filled with mineral oil was utilized to prevent sample evaporation. The shear profile is illustrated in Figure S3. Each shear rate was held around 28 mins and the scattering patterns were collected at the last 10 mins of each shear rate. The applied shear rate in the rheo-SANS experiments (from left to right) are 0.001, 0.005, 0.01, 0.05, 0.1, 0.5, 1, 5, 10, 50, 100 s^{-1}.

Rheology Measurement

Rheological measurements were performed on stress-controlled rheometers (AR-G2 & DHR-1, TA Instrument, New Castle, England) that are equipped with a parallel-plate fixture (diameter = 60 mm, gap size = 1 mm) and solvent trap; all measurements were conducted at 25°C ± 0.1°C. Steady shear measurements were performed at 25°C to record the apparent shear viscosity as a function of increasing shear rate, $\dot{\gamma}$, from 0.005 - 100 s^{-1}. Steady shear viscosity at each shear rate was recorded as the temporal variation of viscosity is within 5%. Thixotropic behavior was measured as the following steps: Three different pre-shear rates, $\dot{\gamma}_{pre} =$ 1, 10 and 100 s^{-1} were applied to individual samples for 3 min to ensure steady shear state. Then, stress was measured at a constant shear rate of $\dot{\gamma}_{\text{measured}} =$ 0.25 s^{-1} right after the pre-shear stopped. Due to the constrained data acquisition time and for better quality of the experimental outcome, the data were collected every 0.5 s. To further investigate the reversibility of the viscosity of the PPR gel, steady-shear experiment was conducted with the following sequence of shear rates: $\dot{\gamma}$ = 0.005, 400, 0.005, 400, 0.005 s^{-1} that were imposed at the onset times of 0, 10, 15, 25, 30, respectively, wherein the time-

evolving apparent viscosity is monitored. Sample appearance before and after these measurements are shown in Figure S4.

Results and Discussion

Hierarchical Structure of PPR Gel in Quiescent State

Figure 1 shows the 1-D scattering pattern obtained from four different techniques including small-angle light scattering (SALS), static light scattering (SLS), small-angle X-ray scattering (SAXS) and wide-angle X-ray scattering (WAXS), covering more than four decades of scattering vector, q. To the best our knowledge, this is the first time that detailed structural characterization of a PPR gel has been resolved from micron to angstrom length scale in a single study, which allows us to reveal four hierarchical structures in the PPR gel.

I. Primary Structure - PPR Crystalline

The WAXS data shown in Figure 1(a) confirms the crystalline structure of PPR. It is known that the channel-type crystalline, in which CD molecules packed in a head-to-head or head-to-tail orientation so that the cavities of CD form infinite channels,[37-39] can be obtained in the PPR self-assembly.[6, 18, 40-42] The diffraction peaks at q = 1.06, 1.42 and 1.57 $Å^{-1}$ stand for the (200), (210) and (300) reflections of the channel-type β-CD crystalline, respectively, while

(100) is not attainable in the WAXS range.[19] The diffraction peak at $q \sim 1.27$ Å^{-1} corresponds to the PEO crystalline structure which has also been reported in a similar system.[15] Other peaks in the WAXS pattern presumably arise from the cage-type crystalline, that the cavity of each β-CD is blocked by adjacent CD molecules on the both sides,[37-39] of β-CD suggesting that not all β-CDs are threaded on the F108 chain. WAXS data not only confirm the successful forming of PPR structure but also suggest a primary structure, which becomes the building block for the other hierarchical morphologies.

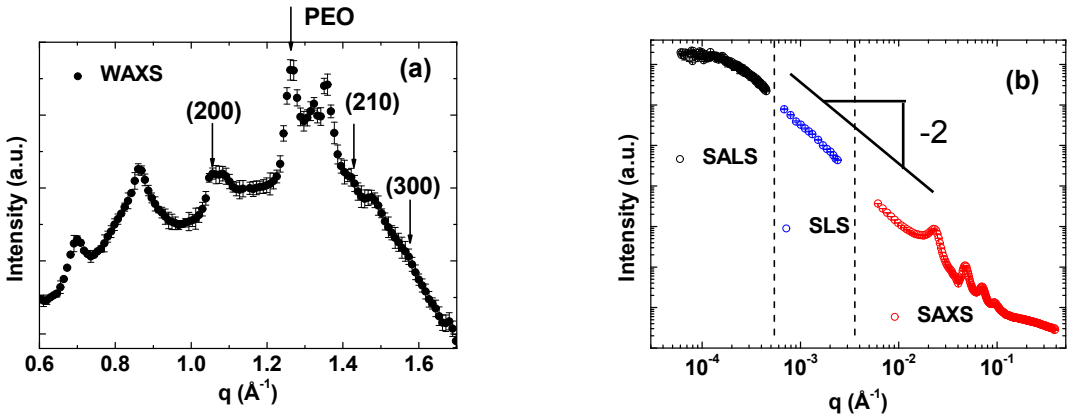

Figure 1. Scattering patterns of the PPR gel measured by (a) WAXS, (b) SALS (black circle), SLS (blue circle) and SAXS (red circle). The arrows in the WAXS pattern indicate the reflection from the channel-type β-CD crystalline.

II. Secondary and Tertiary Structures – Lamellae and Lamellar Stacks

Figure 1(b) presents the scattering pattern obtained from SALS, SLS and SAXS covering a q range from 0.00006 to 0.39 Å^{-1}. A q^{-2} decay between 0.0002 and 0.1 Å^{-1} indicates a characteristic scattering pattern of 2D objects (presumably lamellae). Based on the range of q^{-2} decay, the lateral dimension of the lamellae can be estimated by using $2\pi/q$ which gives us the size ~2-3 μm. According to a previous study,[13] the lamellae are built upon the aforementioned primary structure, channel type β-CD crystalline and are considered as the *secondary* structure. Moreover, the fact that a group of Bragg peaks with high-order harmonics are observed at q^* (at 0.024 Å^{-1}), $2q^*$, $3q^*$ and $4q^*$, corresponding to a long-range highly ordered structure with a d-spacing of 26 nm, suggests that the lamellae pack into lamellar stacks forming the *tertiary* structure. This is consistent with the outcome of a recent study of a self-assembled PPR system with a lamellar d-spacing of 20 nm.[15]

III. Quaternary Structure – Lamellar Stacks Aggregating Grains

The SALS pattern in Figure 1(b) indicates a Guinier-type scattering plateau,[43] where $I(q) \propto \exp\left(-\langle R_g^2\rangle q^2/3\right)$ for $q < 1.2\times10^{-4}$ Å^{-1} with $\langle R_g^2\rangle$ being the mean square of the radius of gyration implying the existence of certain defined morphology. The obtained $\langle R_g^2\rangle^{1/2}$, ~ 700

± 4.5 nm suggests the largest attainable structure in the system. In order to gain more information about the quaternary structure, a confocal laser scanning microscopic (CLSM) experiment is performed on the sample doped with a hydrophobic dye, NR, which is expected to be entrapped in the F108 micelles. The CLSM images (as shown in Figure S5) reveal small dark domains embedded in a continuous red background. The dark domains have an average size of ~ 632 ± 29 nm calculated by the image analysis software,[32] consistent with the $<R_g^2>^{1/2}$ obtained from SALS analysis. Hence, the dark domains are presumably composed of hydrophilic PPR-based structures with little or no NR associated.

A valid question is whether this length scale corresponds to the abovementioned tertiary lamellar stacks? We perform DLS on the PPR gel samples after serial dilution and the results are shown in Figure 2. The more concentrated (five-fold dilution, ~5% solid content) sample indicates two diffusion coefficients resulting in the hydrodynamic radii R_h of ~260 nm and ~ 2300 nm (2.3 μm), respectively, while the other one (30-times dilution, ~0.83% solid content) reveals only the smaller-size particles (*i.e.*, R_h ~260 nm). The structure of the smaller particles remains intact upon dilution and their dimension is much smaller than the bigger

particle and hence unlikely corresponding to the particles with the $<R_g^2>^{1/2}$ obtained from the aforementioned SALS analysis, presumably corresponding to the lamellar stacks. On the contrary, the large aggregates disappear upon dilution, suggesting a weakly-associated quaternary structure, which is more likely representing the "dark domains" in the microscopic images or the particles revealed in SALS. However, the difference between $<R_g^2>^{1/2}$ and R_h is presumably due to strong interparticle hydrodynamic interaction at high concentration. Moreover, the depolarized dynamic light scattering (DDLS) results suggest that the grain is notably anistropic in shape (Figure S6). All the aforementioned evidence indicates that the tertiary lamellar stacks further packed/aggregated into the quaternary structure which will be referred to the "grain" in the following discussion. From the rheo-SANS experiment, we further confirm that the quaternary "grain" is distinct from the tertiary lamellar stacks.

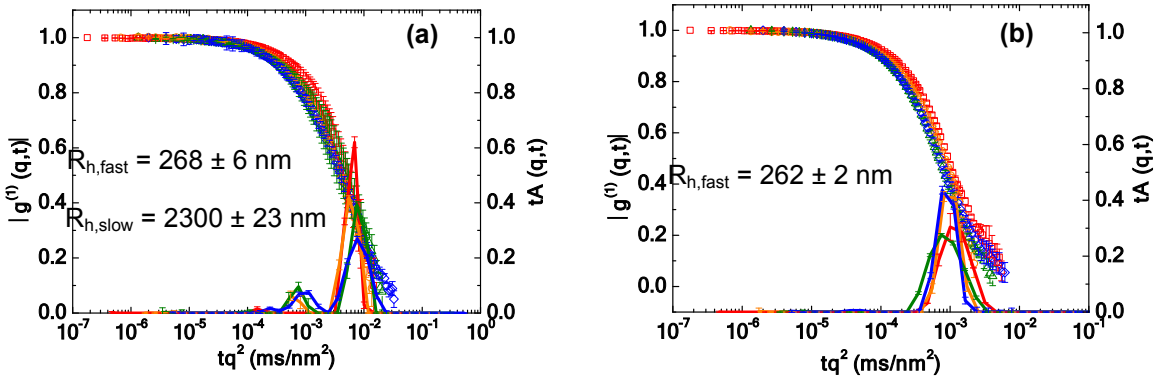

Figure 2. Field autocorrelation functions and the associated decay time distributions extracted from the DLS experiment at scattering angles θ = 30 (red), 60 (orange), 90 (green), and 120 (blue) for the PPR gel diluted by a factor of (a) 5 and (b) 30. The two (fast- and slow-) diffusive modes and the corresponding hydrodynamic radii are marked in each figure. The regularization parameters for CONTIN analysis falls between 10^{-4}–10^{-5}.

The hierarchical structures in the PPR gel are summarized in Scheme 1, wherein the F108 micelles are not depicted for clarity purpose. The grains (the quaternary structure indicated by white arrows) are embedded in the F108 micelles forming the PPR gel [Scheme 1(a)]. The average $\langle R_g^2 \rangle^{1/2}$ of the grains is ~700 nm [Scheme 1(b)]. Each grain is made of several lamellar stacks [tertiary structure Scheme 1(c)] through weak association which can be broken down by dilution. Each lamellar stack is composed of several well-aligned lamellae [Scheme 1(c)] through the sturdy stringing of F108 polymer chains. These lamellae have well-defined *d*-spacing of 26.2 nm [Scheme 1(b)]. Each lamellae (the secondary structure) is composed of channel-type β-CD crystalline [Scheme 1(e)] which was brought together by hydrogen bonding between each β-CD molecule.

(d)

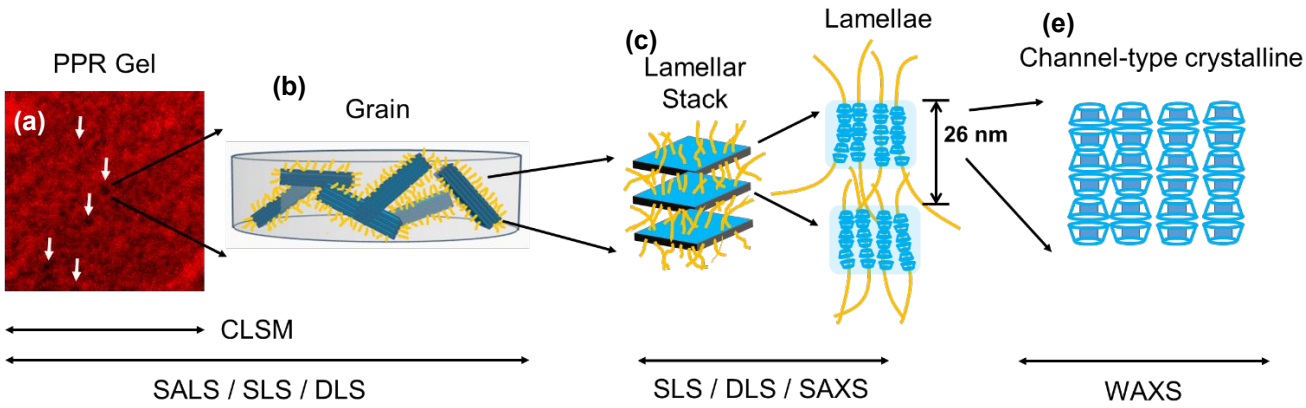

Scheme 1. Hierarchical structures of the PPR gel from the submicron-sized grain to the angstrom crystal structure: (a) CLSM images, (b) sketch for the lamellar stack-rich grain, (c) one lamellar stack, (d) fine structures of the lamellar stack, and (e) the channel-type crystalline of β-CD.

IV. Structure of PPR Gel under Shear Flow

Rheo-SANS experiments were performed to provide detailed structural information of secondary (lamellae) and tertiary (lamellar stacks) PPR gel under shear and during relaxation. The 2-D scattering pattern of F108 was examined first. Isotropic 2-D SANS patterns of F108 micelles were found for either 1-3 or 2-3 scattering plane at any of the applied shear rates (Figure S7), indicating that the F108 micelles are not alignable under shear flow. The scattering ring located at $q \sim 0.04$ Å^{-1} is presumably contributed from the structure factor of the F108 micelle. The 2-D SANS patterns of PPR gel (from both 1-3 and

2-3 scattering planes) are drastically different from those of F108 at the corresponding shear rate as shown in Figure 3. Two scattering rings at $q\sim$ 0.024 and 0.04 Å^{-1} (as indicated by the arrows) can be observed at the 1-3 scattering plane at $\dot{\gamma} = 1$ s^{-1}, [Figure 3(a)] corresponding to the distance of two lamellae in the lamellar stack and the packing of F108 micelle (as discussed above), respectively. The existence of these two rings indicates that the micelle and the lamellar stacks co-exist in the system which is also consistent with the CLSM images (Figure S5). The peak at $q\sim$ 0.024 Å^{-1} diminished and no longer can be observed at $\dot{\gamma} =$ 10 [Figure 3(b)] and 100 [Figure 3(c)] s^{-1}. More structural information is revealed in the rheo-SANS data obtained from the 2-3 scattering plane as shown in Figure 3(d)-(h). All the scattering patterns are highly anisotropic, indicating that the normal of the regular-spaced lamellae as well as the lamellar stacks was in parallel with the velocity gradient. The highest degree of orientation occurs at the highest shear rate of $\dot{\gamma}$ = 100 s^{-1} [Figure 3(f)]. More interestingly, this anisotropy remains even two hours after the shear flow ceases [Figure 3(g)-(h)], implying that the orientation of lamellar structure at such nanoscale is not easily recovered after being aligned (relaxation time τ_1 > 2 hr).

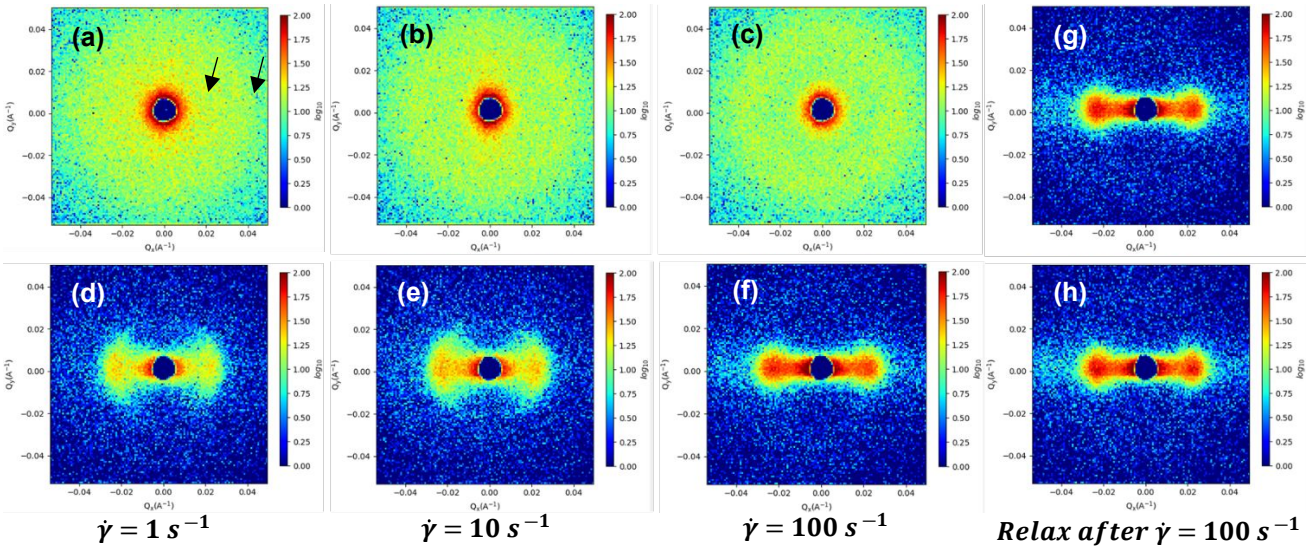

Figure 3. 2-D scattering patterns of PPR gel from the (a-c) 1-3 and (d-h) 2-3 scattering plane at (a & d) $\dot{\gamma}$ = 1, (b & e) 10, (c & f) 100 s^{-1} and (g) right after and (h) after flow cessation for the structure recovery for 2 h. Arrows in (a) indicate the two rings located at q = 0.024 and 0.04 $Å^{-1}$, respectively.

An azimuthal analysis of the peak around q = 0.024 $Å^{-1}$ in the 2-3 scattering plane is shown in Figure S8. The data can be fitted by a double Lorentzian function as given below.

$$I(\chi) = \frac{A}{w^2 + (\chi - \chi_0)^2} + \frac{B}{w^2 + (\chi - \chi_1)^2} + C,$$

where χ, χ_0 and χ_1 are the azimuthal angle and peak positions, respectively. A and B are constants related to peak areas, C is background, w is the peak. The fitting results are summarized in Table 1. It is clear to see that the peak positions barely change with different shear rates and after shear cessation (at ~ 94.0° and ~ 266°), indicating the lamellar normal is along with the velocity gradient direction. The full-width at half maximum (FWHM) also

reveals that the lamellar stacks aligned well not only at the highest shear rate but also after shear cessation. This phenomenon has also been reported in other liquid crystal systems.[44, 45] The Rheo-SANS outcomes reveals the lamellar alignment in the secondary and tertiary structure.

Table 1. The full-width at half maximum (FWHM) of the fitted double Lorentzian peaks. The given uncertainties represent one standard deviation.

Shear Rate (s^{-1})	1	10	100	Relax	Relax (after 2hr)
FWHM	46.6 ± 1.98	46.9 ± 2.12	20.4 ± 0.96	18.8 ± 0.98	18.4 ± 0.96
A	10013 ± 707	12891 ± 1082	5125 ± 381	4951 ± 400	5073 ± 405
B	11706 ± 791	14946 ± 1193	6098 ± 412	5694 ± 445	5862 ± 452
χ_0	93.9 ± 0.71	92.5 ± 0.88	94.5 ± 0.65	94.9 ± 0.68	94.0 ± 0.65
χ_1	267.8 ± 0.64	266.3 ± 0.72	266.5 ± 0.47	266.8 ± 0.56	266.7 ± 0.53
C	-0.28 ± 0.19	-0.76 ± 0.28	-0.09 ± 0.15	-0.11 ± 0.17	-0.15 ± 0.17

SALS measurements were performed to investigate the mesoscale structural evolution (the quaternary structure) of the PPR gel following a short-term stirring. Representative 2-D

scattering patterns and 1-D profiles of SALS measurements are shown in Figure 4. A clear butterfly pattern (with symmetric lobes around the beam center) was observed shortly after the shearing [Figure 4(a)], followed by a less anisotropic pattern after ~ 400 s [Figure 4(b)]. The evolution from anisotropic to isotropic feature suggests that the grains slowly relaxed into a more isotropic orientation and shape after 400 s of quiescence yielding a nearly symmetric 2-D SALS (relaxation time τ_2 < 10 min) pattern in contrast to the un-relaxed, highly anisotropic SANS profile even after 2 hours of equilibrating time. The distinct difference indicates two relaxations: fast in mesoscale (inter-grain) and slow in nanoscale (intra-grain lamellar stacks). This observation is consistent with the aforementioned difference between "grains" and "lamellar stacks" in hierarchical structures. Further analysis on the 1-D scattering curves [Figure 4(c)] suggests that the grain size along the velocity gradient is smaller after relaxation ($<R_g^2>^{1/2}$ ~ 550 nm) compared to that at quiescent state ($<R_g^2>^{1/2}$ ~ 700 nm). This result suggests that the grain size/organization is irreversible after shear force cessation comparing to that in the quiescent state. This might result from the irreversible nanostructural alignment (lamellar normal align with the velocity gradient). Note that the

difference in relaxation time ($\tau_2 << \tau_1$) indicates that the meso-structure has a quicker recovery time than the nano-scale structure.

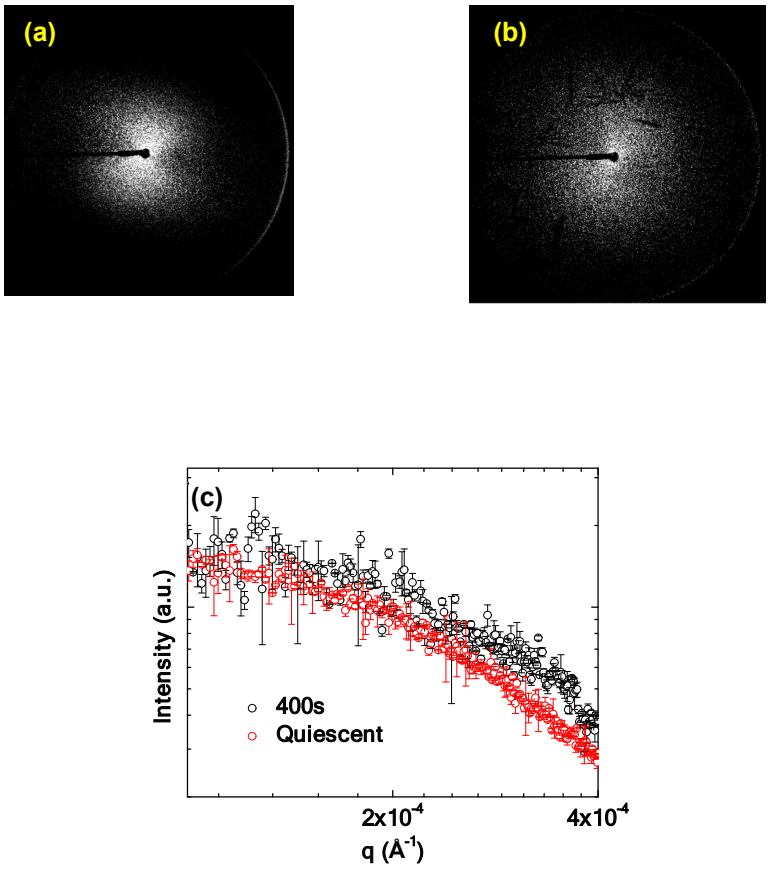

Figure 4. 2-D SALS patterns for the PPR gel at a delayed time of (a) 20 s and (b) 400 s after the treatment of a mild stirring. (c) 1-D SALS patterns for the PPR gel in quiescent state and 400s after shear cessation.

V. Rheological Behavior of PPR Gel

Figure 5(a) shows the steady shear profiles of F108 alone and PPR gel. Newtonian behavior was observed in the F108 solution[4], while shear-thinning behavior could be

observed for the PPR gel. A clear thixotropic phenomenon after applying a lower shear rate ($\dot{\gamma}_{\text{measured}}$) that the shear stress (viscosity) increases as a function of time in all $\dot{\gamma}_{pre}$ applied in the measurement [Figure 5(b)] until a final stress plateau value was reached. It is noteworthy that the higher $\dot{\gamma}_{pre}$ is the lower the final shear stress is. In addition, there is a maximum in the transient stress response at $\dot{\gamma}_{pre} =$ 100 s^{-1}, when the jammed grains yield and start rolling. Moreover, the time-dependent viscosity and stress was measured under the shear history prescribed in [Figure 5(c)] and are reported in [Figure 5(d)] to demonstrate the thixotropic behavior (reversibility of the viscosity) of the PPR gel. At the low-shear-rate intervals (*i.e.*, $\dot{\gamma}$ = 0.005 s^{-1}, steps 1, 3 and 5), although the viscosity is able to build up and reach a plateau within 10 min, the values for the viscosity differs at various intervals. The viscosity obtained in step 1 is higher than step 3 and 5 while the viscosity measured from step 3 and 5 are similar [Figure 5(d)], consistent with the thixotropic behavior and the different dimensions of initial quiescent and after-shear "grains" interpreted from 1-D SALS data [Figure 4 (c)]. In contrast, at the high-shear-rate intervals (*i.e.*, $\dot{\gamma}$ = 400 s^{-1}, steps 2 and 4), the viscosity resumes to a similar and much lower value. In both measurements, we can

see a fast recovery time in the shear stress/viscosity in the time scale of mins. However, the shear stress/viscosity is not able to reach the same value with different pre-shearing conditions of $\dot{\gamma}_{pre}$. Moreover, even by applying the same shear rate ($\dot{\gamma}$ = 400 s^{-1}), the shear stress/viscosity is not able to recover 100% while applying a lower shear rate. Besides, the drop in plateau viscosity between step 1 and step 3 is not comparable for smaller variations in high and low shear-rates as evidenced in Figure 5 (b). The former (high shear) is pertaining to the initial status of grains while the latter (low shear) relates to the "reorganized" grains under different levels of shear.

(a)

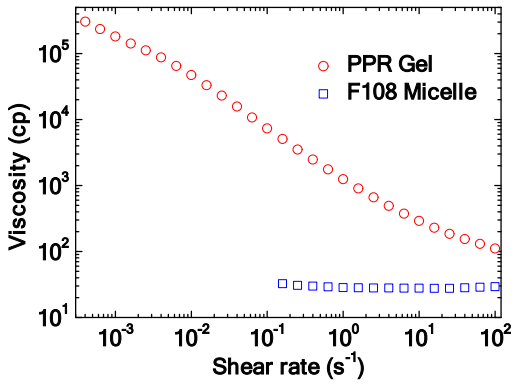

(b)

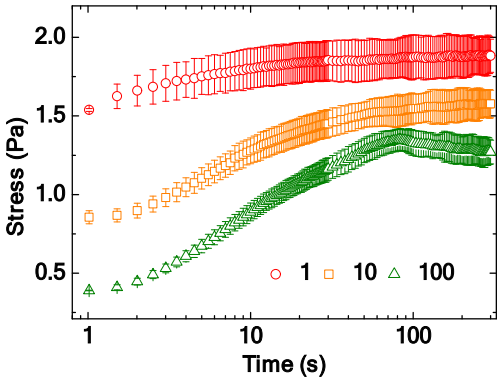

(d)

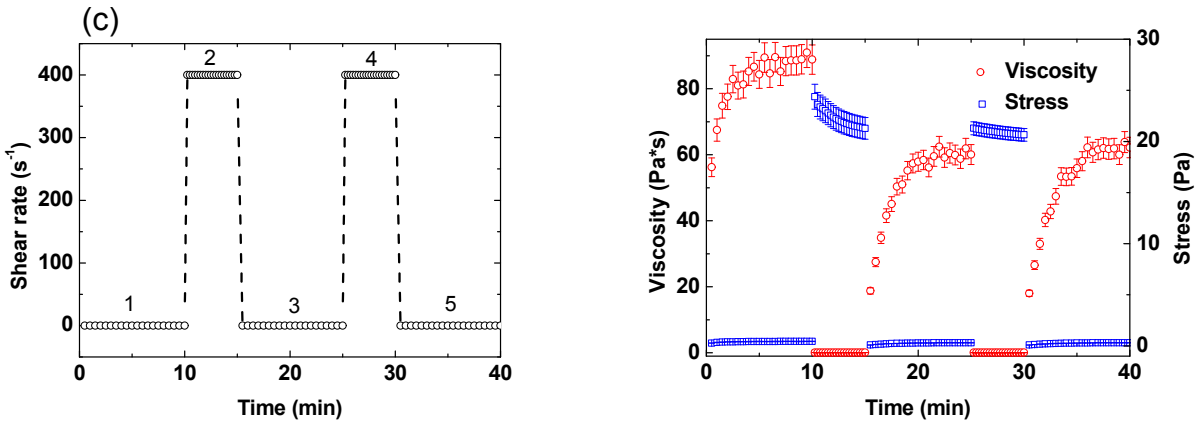

Figure 5. (a) Steady shear flow curves of PPR gel (red circle) and F108 micelle (blue square). (b) Stress response of PPR gel at $\dot{\gamma}_{\text{measured}} =$ 0.25 s^{-1} with different $\dot{\gamma}_{pre}$ =1 (red circle), 10 (orange square) and 100 (green triangle) s^{-1}. (c) Shear profiles as a function of time. The shear profile composed of 5 segments and the details are: $\dot{\gamma}$ = 0.005, 400, 0.005, 400, 0.005 at onset time of 0, 10, 15, 25, 30, respectively. (d) Time-dependent viscosity (red circles) and shear stress (blue squares) response subjected to the shear profile.

VI. Correlation between the Hierarchical Structure and the Rheological Behavior

The rheological behavior can be understood by the proposed hierarchical structure. Prior to the shear disturbance, the orientation of grains and the lamellar stacks is expected to be isotropic as evidenced by SALS and rheo-SANS results [scheme 2(a)]. Here, the lamellae (secondary structure) have the same orientation within one lamellar stack (tertiary structure). The applied shear involved two major structural transformations: orienting the tertiary (lamellar stacks) structure and breaking up (reorganizing) quaternary structure (grains). Both reduced the viscosity of the system. In addition, the observed maximum transient stress at $\dot{\gamma}_{pre} =$ 100 s^{-1} also suggests that the grain size becomes smaller after applied shear which has also been reported previously.[46] The shear aligned lamellar stacks required long time (τ_1) to relax into randomly oriented state [as shown in anisotropic SANS data 2 hours after shear, Figure 3(h)], while the "broken-up" grains reorganized themselves via nearby lamellar stacks into "new" grains relatively fast, τ_2 [as shown in isotropic SALS data 10 mins after shear, Figure 4(b)]. Moreover, different pre-shear rates, $\dot{\gamma}_{pre}$ caused different "initiate" state of the newly organized grains resulting in different initial shear stress (the starting point, t = 1 s) in Figure 5(b). As a result, lower $\dot{\gamma}_{pre}$ yields

higher initial shear stress. The fast recovery of the shear stress/viscosity is in the time scale comparable to the grain relaxation (τ_2) [Figure 4(b) & 5(b)], suggesting that the grain reorganization should be mainly responsible for the thixotropy of PPR gel as evidenced by a previous study.[47] On the contrary, the dependence of plateau shear stress (and plateau viscosity) on $\dot{\gamma}_{pre}$ in Figure 5(d) suggests different "final structures" of the grains since the relaxation time of lamellar stacks (τ_1) is longer than 2 h [Figure 3(g) & (h) & scheme 2(b)]. To summarize, a reorganization of grains with aligned lamellar stacks regrouped upon shear [scheme 2(b)] and a fast re-organization of grains upon the cease of flow might take place in spite of the slow intra-grain relaxation of lamellar orientation over a long period of time (hours if not days) after shear [Figure 3(f)-(h) & scheme 2(c)].

(a)

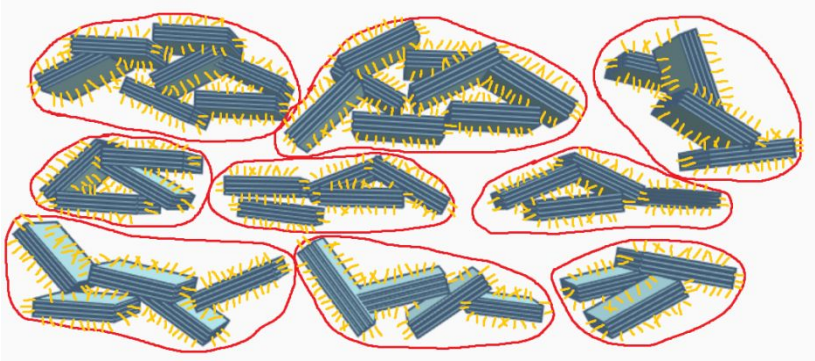

(b)

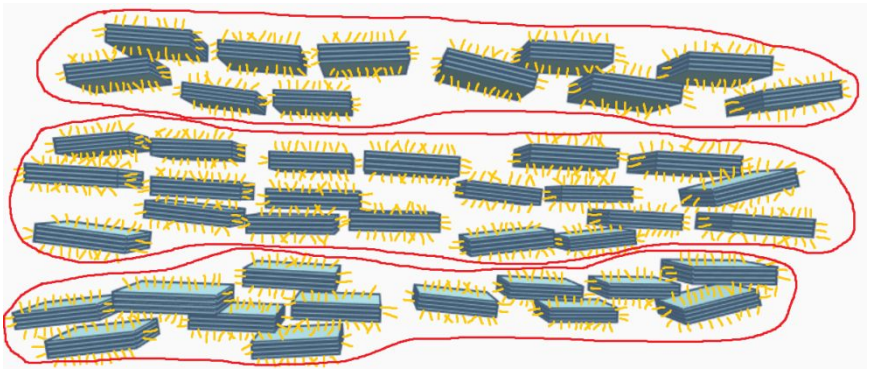

(c)

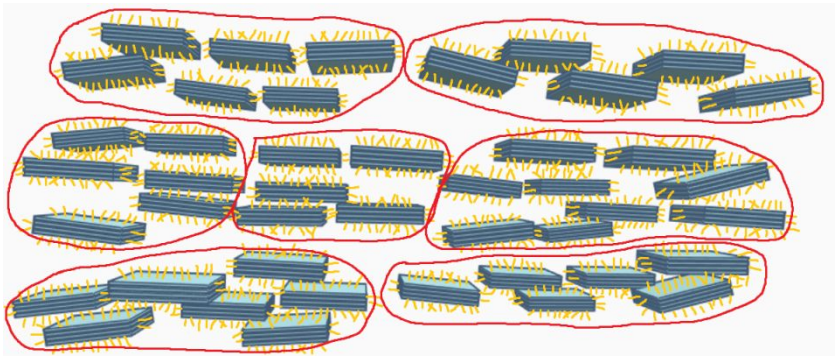

Scheme 2. Schematic representation of the (a) isotropically distributed grains and lamellar stacks in the quiescent state, (b) aligned lamellar stacks in the aligned grains subjected to shear flow and (c) grains are slowly relaxed into less anisotropic shape and are less oriented after shear for a period of time but may not fully recover to be isotropic in shape and orientation. Within one lamellar stack (tertiary structure), the lamellae (secondary structure) have the same orientation. The yellow lines represent F108 molecules, the blue stacks are the lamellar stacks (the tertiary structure) as described in scheme 1 and the red lines are the boundary of the "grains" (the quaternary structure).

Conclusions

Here, we report that the hierarchical structures of a PPR gel (obtained via SALS, SAXS, SANS and WAXS) are closely related to its rheological behavior. The primary structure is composed of channel-type crystalline of β-CDs, which further self-assemble into the secondary structure, lamellae. The strong stringing of F108 polymer chains yields the tertiary structure, lamellar stacks with a well-defined *d*-spacing. These lamellar stacks are then weakly associated with each other forming the microscopic grains. Significant effects of shear flow on structural transformations include orientation/alignment of lamellar stacks and reorganization of grains. The rheological responses correspond to the proposed structural transformation well. The relaxation of nanoscale lamellar alignment is slow (hours or days) compared to that of the mesoscale grain reorganization (minutes) after shear flow ceases. Thixotropy of the PPR gel has been identified to stem principally from the reorganization of grains. Higher shear rate yields better lamellar alignment, tears down the grain and regroups (reorganizes) the lamellar stacks into new grains. The newly equilibrating structure of grains dictates the initial viscosity of sheared

PPR. This study provides new insight into the structure-rheology relationship for the PPR system in general.

Conflicts of interest

There are not conflicts of interest.

Acknowledgement

This work was supported by the Grant 102-2313-B-002-056-MY3 and 105-2917-I-002-025- from the Ministry of Science and Technology (MOST), Taipei, Taiwan. Certain commercial equipment, instruments, or materials (or suppliers, or software etc.) are identified in this paper to foster understanding. Access to NGB 30m SANS was provided by the Center for High Resolution Neutron Scattering (CHRNS), a partnership between the NIST and the National Science Foundation (NSF) under Agreement No. DMR-1508249. Such identification does not imply recommendation or endorsement by the National Institute of Standards and Technology (NIST), nor does it imply that the materials or equipment identified are necessarily the best available for the purpose.

1. I. W. Hamley, *The Physics of Block Copolymers*, Oxford University Express, New York, 1998.
2. P. Alexandridis, T. Nivaggioli and T. A. Hatton, *Langmuir*, 1995, **11**, 1468-1476.
3. P. Alexandridis, J. F. Holzwarth and T. A. Hatton, *Macromolecules*, 1994, **27**, 2414-2425.
4. R. K. Prud'homme, G. Wu and D. K. Schneider, *Langmuir*, 1996, **12**, 4651-4659.
5. I. W. Hamley, *The Physics of Block Copolymers*, Oxford University Express, New York, 1998.
6. J. Li, X. Ni, Z. Zhou and K. W. Leong, *J. Am. Chem. Soc.*, 2003, **125**, 1788-1795.
7. J. Szejtli, in *Comprehensive Supramolecular Chemistry*, eds. J. Szejtli and T. Osa, Pergamon, New York, 1996, vol. 3, ch. 2, pp. 13-16.
8. J. Joseph, C. A. Dreiss, T. Cosgrove and J. S. Pedersen, *Langmuir*, 2007, **23**, 460-466.
9. C. A. Dreiss, E. Nwabunwanne, R. Liu and N. J. Brooks, *Soft Matter*, 2009, **5**, 1888-1896.
10. M. Valero and C. A. Dreiss, *Langmuir*, 2010, **26**, 10561-10571.
11. C. Perry, P. Hebraud, V. Gernigon, C. Brochon, A. Lapp, P. Lindner and G. Schlatter, *Soft Matter*, 2011, **7**, 3502-3512.
12. J. Qin, X. W. Meng, B. J. Li, W. Ha, X. Q. Yu and S. Zhang, *J. Colloid Interface Sci.*, 2010, **350**, 447-452.
13. K. C. Shih, C. Y. Li, W. H. Li and H. M. Lai, *Soft Matter*, 2014, **10**, 7606-7614.
14. J. Huang, Z. Y. Zhou, M. Wei, Y. Chen and P. R. Chang, *J. Appl. Polym. Sci.*, 2008, **107**, 409-417.
15. S. Uenuma, R. Maeda, H. Yokoyama and K. Ito, *Chem. Commun.*, 2019, **55**, 4158-4161.
16. J. Wang and X. T. Zhang, *Acs Nano*, 2015, **9**, 11389-11397.
17. K. M. Huh, Y. W. Cho, H. Chung, I. C. Kwon, S. Y. Jeong, T. Ooya, W. K. Lee, S. Sasaki and N. Yui, *Macromol. Biosci.*, 2004, **4**, 92-99.
18. H. S. Choi, K. Kontani, K. M. Huh, S. Sasaki, T. Ooya, W. K. Lee and N. Yui, *Macromol. Biosci.*, 2002, **2**, 298-303.

19. K. M. Huh, T. Ooya, W. K. Lee, S. Sasaki, I. C. Kwon, S. Y. Jeong and N. Yui, *Macromolecules*, 2001, **34**, 8657-8662.
20. J. Li, X. Li, X. P. Ni, X. Wang, H. Z. Li and K. W. Leong, *Biomaterials*, 2006, **27**, 4132-4140.
21. G. Gonzalez-Gaitano, M. A. da Silva, A. Radulescu and C. A. Dreiss, *Langmuir*, 2015, **31**, 5645-5655.
22. M. Micutz, E. Matalon, T. Staicu, D. Angelescu, A. M. Ariciu, A. Rogozea, I. M. Turcu and G. Ionita, *New J. Chem.*, 2014, **38**, 2801-2812.
23. C. Pradal, K. S. Jack, L. Grondahl and J. J. Cooper-White, *Biomacromolecules*, 2013, **14**, 3780-3792.
24. X. Li and J. Li, *J. Biomed. Mater. Res., Part A*, 2008, **86A**, 1055-1061.
25. J. Mewis and N. J. Wagner, *Adv. Colloid Interface Sci.*, 2009, **147-148**, 214-227.
26. M. J. Armstrong, A. N. Beris, S. A. Rogers and N. J. Wagner, *J. Rheol.*, 2016, **60**, 433-450.
27. Z. Liu, G. Xu, C. Wang, C. Li and P. Yao, *Int. J. Pharm.*, 2017, **530**, 53-62.
28. J. Li, X. Li, X. Ni, X. Wang, H. Li and K. W. Leong, *Biomaterials*, 2006, **27**, 4132-4140.
29. J. Li, *NPG Asia Mater.*, 2010, **2**, 112-118.
30. V. Ajay Mallia and R. G. Weiss, *Soft Matter*, 2016, **12**, 3665-3676.
31. R. H. Guo, C. H. Hsu, C. C. Hua and S. A. Chen, *J. Phys. Chem. B*, 2015, **119**, 3320-3331.
32. J. Schindelin, I. Arganda-Carreras, E. Frise, V. Kaynig, M. Longair, T. Pietzsch, S. Preibisch, C. Rueden, S. Saalfeld, B. Schmid, J. Y. Tinevez, D. J. White, V. Hartenstein, K. Eliceiri, P. Tomancak and A. Cardona, *Nat. Methods*, 2012, **9**, 676-682.
33. Y. H. Wen, P. C. Lin, C. C. Hua and S. A. Chen, *J. Phys. Chem. B*, 2011, **115**, 14369-14380.
34. H. L. Yi, C. H. Wu, C. I. Wang and C. C. Hua, *Macromolecules*, 2017, **50**, 5498-5509.

35. C. J. Glinka, J. G. Barker, B. Hammouda, S. Krueger, J. J. Moyer and W. J. Orts, *J. Appl. Crystallogr.*, 1998, **31**, 430-445.
36. S. R. Kline, *J. Appl. Crystallogr.*, 2006, **39**, 895-900.
37. D. MacNicol, J. Davies and J. Atwood, *Inclusion compounds*, Academic Press, 1984.
38. W. Saenger, *Isr. J. Chem.*, 1985, **25**, 43-50.
39. W. Saenger and T. Steiner, *Acta Crystallogr., Sect. A: Found. Crystallogr.*, 1998, **54**, 798-805.
40. A. Harada, M. Okada, J. Li and M. Kamachi, *Macromolecules*, 1995, **28**, 8406-8411.
41. J. Li, B. Chen, X. Wang and S. H. Goh, *Polymer*, 2004, **45**, 1777-1785.
42. Y. A. Gao, Z. H. Li, J. M. Du, B. X. Han, G. Z. Li, W. G. Hou, D. Shen, L. Q. Zheng and G. Y. Zhang, *Chem. - Eur. J.*, 2005, **11**, 5875-5880.
43. A. Guinier, *Ann. Phys. (Paris)*, 1939, **12**, 161-237.
44. S. Paasch, F. Schambil and M. J. Schwuger, *Langmuir*, 1989, **5**, 1344-1346.
45. J. M. Franco, J. Munoz and C. Gallegos, *Langmuir*, 1995, **11**, 669-673.
46. M. Dinkgreve, M. Fazilati, M. Denn and D. Bonn, *J. Rheol.*, 2018, **62**, 773-780.
47. J. C. W. Lee, K. M. Weigandt, E. G. Kelley and S. A. Rogers, *Phys. Rev. Lett.*, 2019, **122**.

Table of Contents (TOC) graphic

The reorganization of meso-structured “clusters”, is composed of multiple lamellar stacks strung by F108, yielding the thixotropic property.

Quiescent State After Shear